Area Code: 6

Exploring the Scope of Multiband Detection with Next-Generation Gravitational Wave Detectors

A Dissertation Submitted
in Partial Fulfilment of the Requirements
for the

MINOR DEGREE

in

DATA SCIENCE

by

Akshita Mittal
(Roll No. IMS19027)

to

SCHOOL OF DATA SCIENCE
INDIAN INSTITUTE OF SCIENCE EDUCATION AND RESEARCH
THIRUVANANTHAPURAM - 695 551, INDIA

April 2023

DECLARATION

I, **Akshita Mittal (Roll No: IMS19027)**, hereby declare that, this report entitled **"Exploring the Scope of Multiband Detection with Next-Generation Gravitational Wave Detectors"** submitted to Indian Institute of Science Education and Research, Thiruvananthapuram towards the partial requirement of **Minor Degree** in **Data Science**, is an original work carried out by me under the supervision of **Dr Apratim Ganguly and Dr Shabnam Iyyani**, and has not formed the basis for the award of any degree or diploma, in this or any other institution or university. I have sincerely tried to uphold academic ethics and honesty. Whenever a piece of external information or statement or result is used then, that has been duly acknowledged and cited.

Thiruvananthapuram - 695 551 **Akshita Mittal**
April 2023

CERTIFICATE

This is to certify that the work contained in this project report entitled **"Exploring the Scope of Multiband Detection with Next-Generation Gravitational Wave Detectors"** submitted by **Akshita Mittal** (**Roll No: IMS19027**) to Indian Institute of Science Education and Research, Thiruvananthapuram towards the partial requirement of **Minor Degree** in **Data Science** has been carried out by her under my supervision and that it has not been submitted elsewhere for the award of any degree.

Thiruvananthapuram - 695 551
April 2023

Dr Apratim Ganguly
Project Co-supervisor

Dr Shabnam Iyyani
Project Co-supervisor

ACKNOWLEDGEMENT

This report not only represents my work at the keyboard but is also proof that collaborations across institutes lead to fruitful research. I am indebted to Dr Apratim Ganguly and Ms Kanchan Soni for regularly meeting with me and guiding the course of this project. I am grateful to Dr Shabnam Iyyani for agreeing to be my faculty advisor at IISER and for making this collaboration possible. I am also thankful to her for making me a part of her research group and giving me my first experience of an in-person research group meeting.

I would like to extend a special thanks to Kanchan for making time outside the schedule of this project, corresponding with me even on the weekends and driving the project to its completion. I am lucky to have a mentor like you.

I am lastly grateful to the Indian Institute of Science Education and Research Thiruvananthapuram for providing the necessary resources and facilities to complete this project to the best of my ability.

Thiruvananthapuram - 695 551 **Akshita Mittal**
April 2023

ABSTRACT

Black holes are broadly classified into three categories– stellar mass, intermediate mass, and supermassive. LIGO and Virgo have detected gravitational waves from multiple mergers of stellar-mass black holes, however, none have been detected for heavier black hole systems. The mergers of heavier systems are not *loud* enough in current ground-based detectors' hecto-hertz frequency band. The heaviest merger observed by the twin LIGO and Virgo collaborations is GW190521, with final mass $150M_{\odot}$. With the Laser Interferometer Space Antenna (LISA) soon to be operational in the milli-hertz band, we propose an observatory most sensitive in the deci-hertz band, which will bridge the gap between the LISA and LIGO frequency bands. This proposed observatory will be most sensitive in 0.1Hz-1Hz, offering promising observations for mergers that have remained elusive thus far. This work explores the prospects of multiband detection with the next-generation LIGO and our proposed deci-hertz observatory working together. We conduct this study by generating a black hole population and conducting zero-noise injections, followed by a detailed analysis of their signal-to-noise ratios (SNRs) in the respective bands. We observe that the proposed deci-hertz observatory has a detectability of 100% and outperforms the current hecto-hertz detectors significantly.

Keywords: *Gravitational waves, multiband detection, deci-hertz, matched filtering, signal injection*

Contents

List of Figures

List of Tables

1 Introduction

1.1 Objective and Research Question

The aim of this project is to explore the detection capabilities of proposed next generation gravitational wave detectors. The deci-hertz frequency range is expected to be populated with heavier-mass black holes. We also explore the prospects of a system of multiband detectors, laying the groundwork for the detection of signals from binary systems populating the deci-hertz band.

1.2 Motivation

The first detection of gravitational waves from a stellar-mass black hole system in 2015 paved the way for exciting research and presented us with an opportunity to probe the universe for questions that form the foundation of physics [1]. This observation was the first of many made by the LIGO and Virgo collaborations (HLV). We have observed $\sim$ 90 mergers to date [2]. However, gravitational wave signals from bigger black holes have remained elusive thus far, owing to their higher component masses. Heavier-mass black holes, when detected, will have a host of implications for information about the population distribution and formation channels for these sources.

The detection of a signal from heavier-mass BH systems is limited by the sensitivity of the presently operational ground-based detectors twin-LIGO and Virgo. These detectors are most sensitive in the hecto-hertz range, i.e., $\sim$ 100Hz, making them optimal for detecting signals from stellar mass candidates.

The frequency at which a BBH merger signal reaches its maximum varies inversely with the binary's total mass. For GW190521 [3], the heaviest BBH merger detected to date, this peak occurred at $\sim$ 60Hz, much lower than that for GW150914, where the peak was at $\sim$ 150Hz — well within in the operational range of LIGO. Similarly, the time that a BBH signal spends in the sensitivity band of these ground-based detectors is inversely proportional to the total mass of

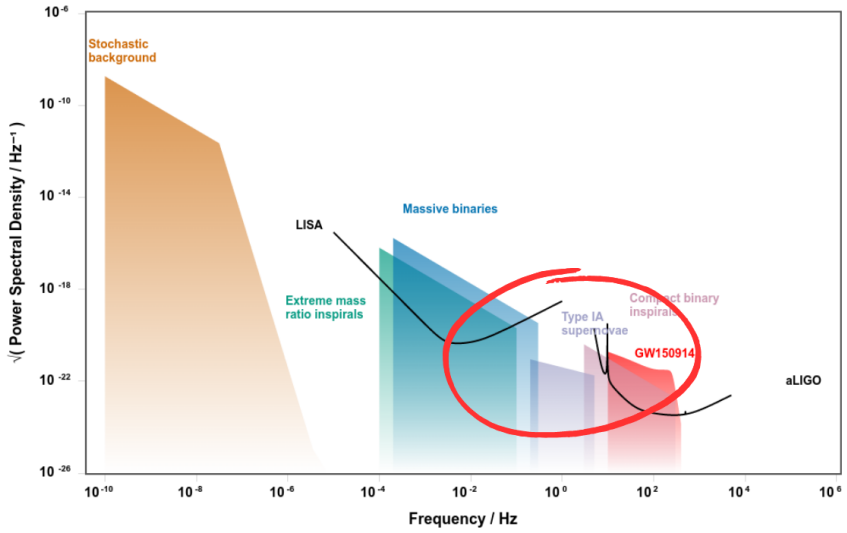

Figure 1.1: Illustration of frequency bands with current and proposed detectors. Highlighted region in red is the frequency band for the proposed deci-hertz detector. Made using GWPlotter [5].

the system. This signal lasted only for $\sim$ 0.1s for GW190521. A new generation of detectors that operate at a lower frequency than the current detectors will help us probe the universe for heavier-mass binary black hole systems.

A deci-hertz detector, with sensitivity in the frequency band 0.1-100Hz, is one such proposed instrument. With the upcoming Laser Interferometer Space Antenna, popularly known as LISA [4], most sensitive in the milli-hertz range, a deci-hertz observatory will bridge the gap between the milli and hecto bands (Figure 1.1), increasing the chances of detection of signals from BBH mergers with heavier component masses. Both these are space-based observatories, which is why their sensitivity is not limited by noise sources that limit the sensitivity of ground-based detectors, allowing them to operate in a much lower frequency range. Moreover, space-based detectors will allow observation of the initial stages of a binary merger, potentially providing us with more information about the sources.

These next-generation detectors, working in conjugation with ground-based detectors will enable us to *listen* to sources with component masses heavier than

stellar mass sources. In this work, we explore the scientific potential of multiband observations of black holes with a deci-hertz observatory and hecto-hertz observatories, HLV. We conduct this study by creating a population of black holes using the `bilby` package [6], conducting zero-noise signal injections, following which, we analyze the SNRs obtained for each signal in the deci and hecto bands. We aim to explore the underlying population distribution of the compact binary parameters in the deci-hertz band using predictive analysis.

2 Listening to the Cosmos: The Science of Gravitational Wave Detection

The detection and analysis of gravitational waves provide unprecedented insights into some of the most extreme phenomena in the Universe, including black hole mergers, neutron star collisions, and the birth of new gravitational wave sources. The process of detecting gravitational waves involves monitoring the distance between two objects, known as interferometers, to measure the minute changes in the fabric of spacetime caused by passing gravitational waves. These measurements are then analyzed using sophisticated signal processing algorithms, which extract the relevant information from the noisy data.

2.1 Understanding Gravitational Waves

A gravitational wave has two independent states of polarization as per Einstein's theory: the plus polarization (h_+) and the cross polarization ($h_\times$). Simply defined, polarization is the geometric shape of the stretching and squeezing of space-time caused by a gravitational wave as it moves, which justifies the naming convention of gravitational-wave polarizations.

2.1.1 Signal Composition

A general gravitational-wave signal (h) can be represented as a linear combination of its polarizations.

$$h = A_+ h_+ + A_\times h_\times \tag{2.1}$$

where A_+ and $A_\times$ are the pattern functions for a detector.

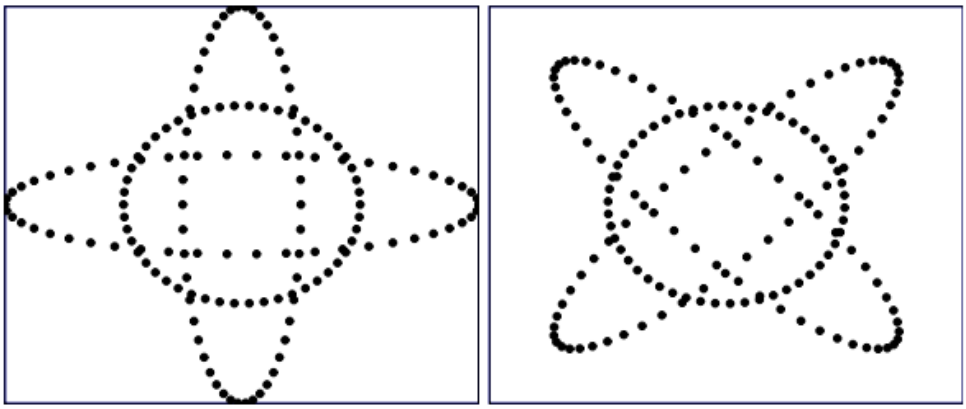

Figure 2.1: Image taken from [7], left shows the effect of a plus-polarized wave in the z-direction on test particles in a circular ring in the (x, y)-plane, while right shows the effect of a cross-polarized wave on the same system.

However, because of the multiple noise sources present (discussed in section 2.4), the output of any observatory is not just the gravitational-wave signal, instead, it comprises the gravitational-wave signal ($h(t)$) and some noise ($n(t)$).

$$s(t) = h(t) + n(t) \tag{2.2}$$

This data obtained from the detectors have to be processed to get rid of the noise so that the signal can be *heard* clearly.

2.2 Types of Gravitational Wave Sources

The types of sources that produce gravitational waves range from the most violent and energetic events in the Universe, such as compact binary coalescences (CBCs), to more mundane sources such as the motion of orbiting objects. Another source of gravitational waves is the stochastic gravitational wave background, a faint and nearly uniform background of gravitational waves that permeates the Universe. This work focuses on gravitational waves from binary black hole systems.

2.3 Gravitational Wave Interferometers

Gravitational wave interferometers typically consist of two or more arms that are arranged in an L-shaped configuration. The basic working principle of a grav-

itational wave interferometer involves the use of lasers and mirrors to measure extremely small changes in the distance caused by passing gravitational waves. A laser beam is split and sent down each arm of the interferometer, where it bounces off a mirror and returns to the central beam splitter. When the two laser beams recombine at the beam splitter, they create an interference pattern that can be measured and analyzed to detect changes in the distance between the mirrors. This change in the length of the arms is reflected as *strain*. To detect gravitational waves, interferometers need to be highly isolated from external vibrations and other sources of noise that could interfere with the measurement. They are typically housed in large vacuum chambers to minimize the effects of noise, which is the main factor limiting the sensitivity of these detectors.

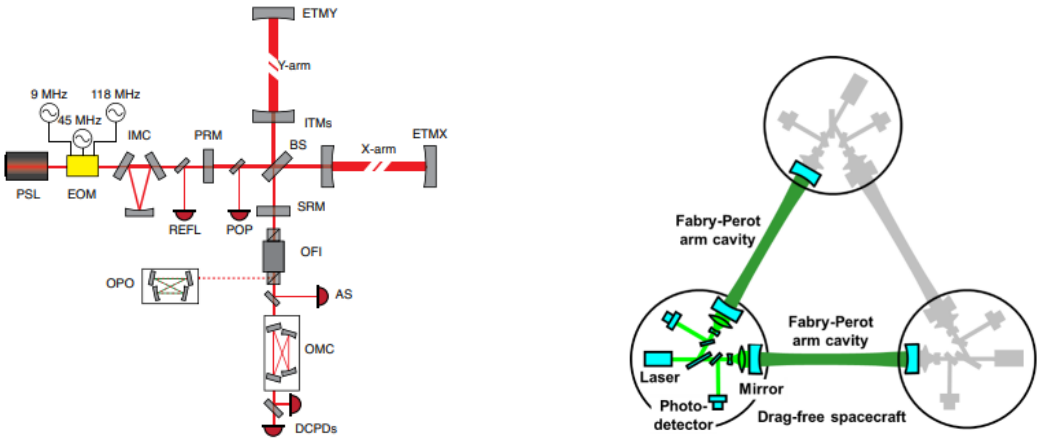

Figure 2.2: Layout of an Advanced LIGO detector for O3 (left) [8]. Design of one cluster of a deci-hertz observatory (right) [9].

2.4 Sources of Noise

The distortion is space-time caused by a gravitational wave passing through is of the order of 10^{-21}m. Given this small order of magnitude, it is essential that the main sources of noise are dealt with. The main sources of noise for ground-based detectors are thermal noise and quantum noise.

2.4.1 Thermal Noise

Thermal noise is a fundamental limitation for gravitational wave detectors, arising from the random thermal motion of the atoms that make up the detector's

materials. This noise is a source of uncertainty in the detector's output and can mask weak gravitational wave signals. The level of thermal noise is dependent on the temperature of the detector, with higher temperatures leading to increased thermal noise. To mitigate this noise, gravitational wave detectors are operated at cryogenic temperatures, typically at or near absolute zero, which minimizes the thermal motion of the atoms and reduces the associated noise. Additionally, the materials used in the construction of the detector must be carefully chosen for their low thermal noise properties.

2.4.2 Quantum Noise

Quantum noise is another fundamental limitation for gravitational wave detectors, arising from the Heisenberg uncertainty principle, which places a fundamental limit on the precision with which certain physical quantities can be measured. In the case of gravitational wave detectors, this uncertainty manifests as fluctuations in the phase and amplitude of the laser light used to measure the tiny ripples in space-time caused by passing gravitational waves. These fluctuations can be significant enough to mask the gravitational wave signal, particularly at high frequencies. To mitigate quantum noise, gravitational wave detectors use a variety of techniques, including squeezing the laser light to reduce the quantum noise in one of the measured quadratures and using high laser powers and long interaction times to improve the signal-to-noise ratio.

2.4.3 Shot Noise

Shot noise arises due to the discrete nature of photons, the particles of light that are used to measure the tiny ripples in space-time caused by gravitational waves. The number of photons detected by the detector is inherently random and subject to statistical fluctuations. These fluctuations result in an uncertainty in the detector's output, which can shadow the weak gravitational wave signal. Shot noise can be reduced by increasing the intensity of the laser light used in the detector, which increases the number of photons detected, or by using more sensitive detectors that are capable of detecting smaller numbers of photons. However, increasing the laser power also increases other types of noise, such as thermal noise and quantum noise, which must be carefully balanced against shot noise to achieve the best possible sensitivity.

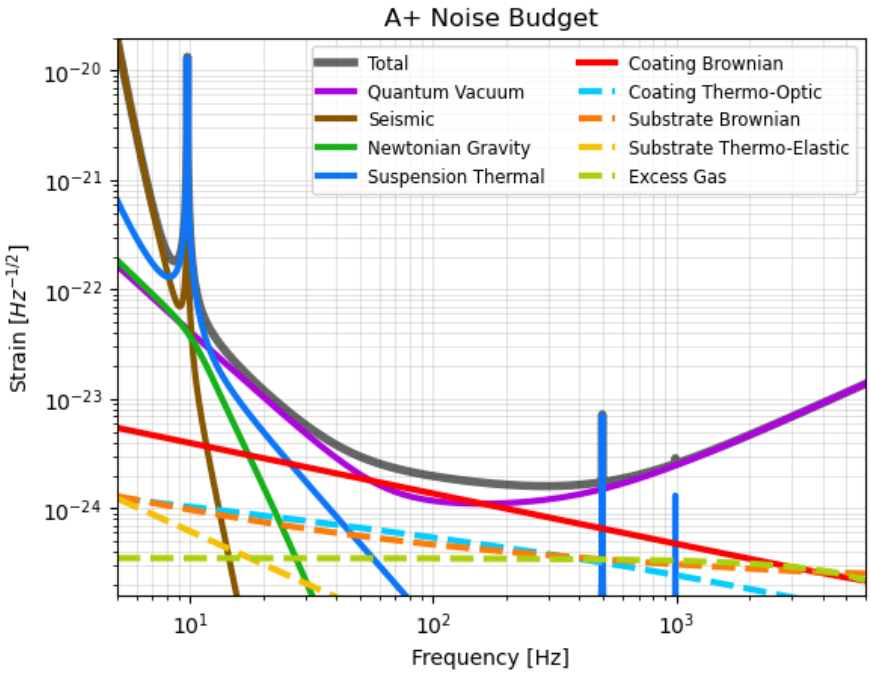

Figure 2.3: Noise budget for A+ evaluated using Gravitational Wave Interferometer Noise Calculator (GWINC). [10]

2.5 Sensitivity Curves

The main component that characterizes the performance of a gravitational wave detector is the *power spectral density* (PSD) of its noise background. From (2.2), the signal output of a detector is just noise in the absence of a signal. The PSD for HLV are obtained from LIGO DCC [11]. The PSD for the hypothetical deci-hertz observatory is empirically determined. For frequency f_{deci}, the power spectral density for the deci-hertz observatory is

$$S_n^{deci} = (10^{-25} f_{deci}^{-2} + 10^{-24} f_{deci}^{1} + 10^{-23} f_{deci}^{0})^2 \tag{2.3}$$

The Python script for the execution of this can be found here [12].

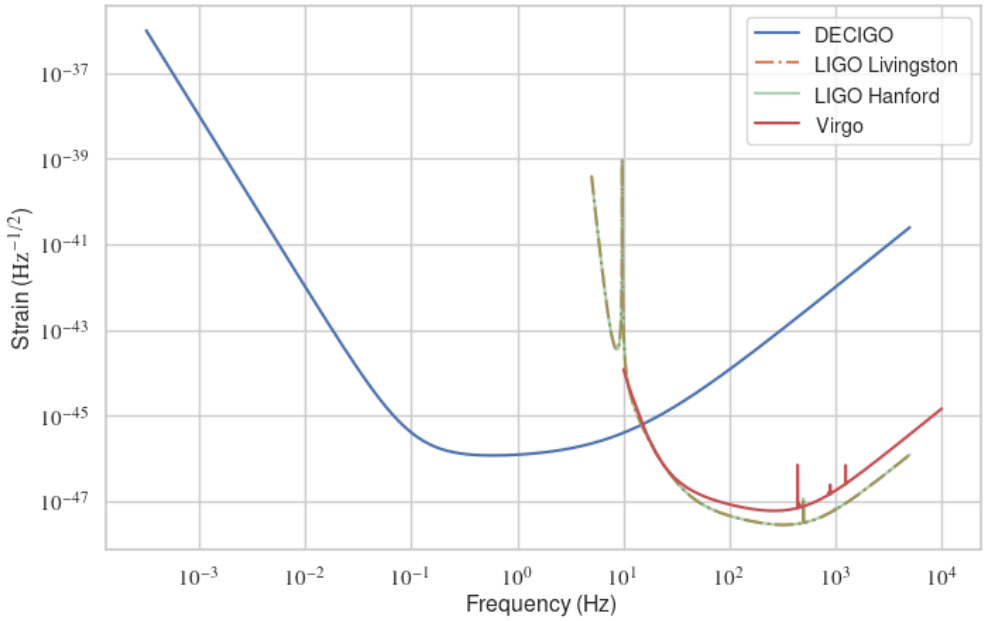

Figure 2.4: Theoretical PSDs for LIGO Hanford, LIGO Livingston, Virgo and our proposed deci-hertz observatory. Data for LIGO+Virgo obtained from A+ Design Curves [11].

2.5.1 Power Spectral Density

Assuming a stationary noise background, the noise $n(t)$ can be fully represented by the one-sided noise PSD $S_n(f)$

$$\langle \tilde{n}(f)\tilde{n^*}(f)\rangle = \frac{1}{2}\delta(f-f')S_n(f) \tag{2.4}$$

Noise is measured over a long duration T, after which its Fourier transform is computed with a frequency resolution $\Delta f = T^{-1}$. The noise PSD $S_n(f)$ has units of inverse frequency. Another commonly used quantity is the *amplitude spectral density*, which is the square root of the PSD and has dimensions of $\mathrm{Hz}^{-1/2}$. ASD is the most frequently plotted quantity in literature.

To make data analysis easier, the noise PSD is assumed to be infinite below a certain frequency cutoff (f_c). Analytical form of PSDs for the LIGO and the deci-hertz detectors is provided in Table 2.1.

Detector	f_c	PSD
aLIGO	20	$x^{-4.14} - 5x^{-2} + \frac{111(1-x^2+0.5x^4)}{1+0.5x^2}$
Virgo	20	$(7.8x)^{-5} + 2x^{-1} + 0.63 + x^2$
Deci-hertz detector	0.05	$(10^{-25} f_{deci}^{-2} + 10^{-24} f_{deci}^{1} + 10^{-23} f_{deci}^{0})^2$

Table 2.1: Analytical forms of power spectral density for aLIGO and Virgo taken from [7]. $x = f/f_0$ where $f_0 = 215$ for aLIGO and $f_0 = 500$ for Virgo.

2.6 Post Merger Analysis

After each observing run of the LIGO+Virgo detectors, extraction of the signal from the noise is done using numerical methods. The data obtained can further be used to estimate the parameters of the source, conduct tests of general relativity or calibrate the detectors. The numerical methods employed for this data handling are discussed in detail in chapter 3.

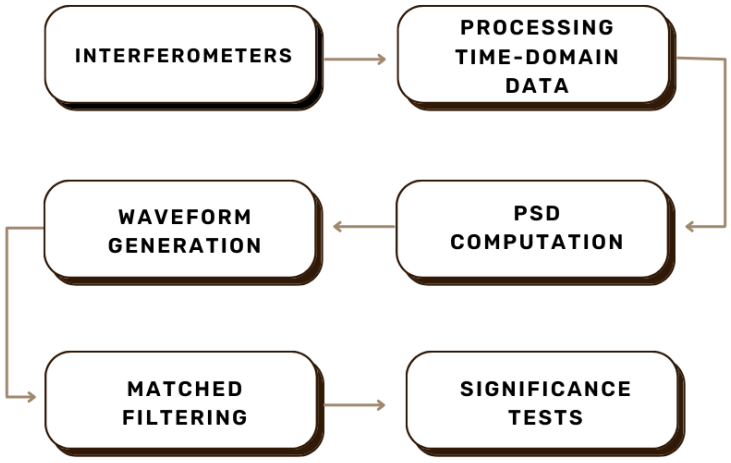

Figure 2.5: Representation of a general data analysis flow in gravitational wave data analysis. Image created using Canva.

3 Post Merger Data Analysis

Gravitational-wave detectors collect multitudes of data throughout their observing runs. However, this data needs to be processed using numerical methods to ascertain the presence of real gravitational-wave signals in it. The gravitational wave data processing methods discussed here include the work carried out for the scope of the project.

3.1 Object-Oriented Programming

Object-oriented programming (OOP) is a programming paradigm that allows for the creation of reusable and modular code. In the context of data science, OOP can be used to build robust and scalable data processing pipelines, as well as to create and manage complex data models. By encapsulating data and functionality within objects, OOP can help to reduce code complexity and improve code maintainability. Additionally, OOP principles such as inheritance and polymorphism can be used to facilitate the creation of flexible and extensible data models. `GWPy` and `PyCBC` are two such Python packages designed for gravitational-wave data analysis that utilise OOP principles to provide a modular and reusable codebase.

3.2 Processing Time-Domain Data

The output of gravitational-wave detectors is a time series of data representing the strain induced by the gravitational wave. This data must be transformed into the frequency domain using Fourier transform. Fourier transform decomposes the time-domain signal into its constituent frequencies, allowing the identification of the frequency components that make up the signal. The resulting frequency-domain data can then be analyzed using various signal processing techniques, including matched filtering, spectrograms, and wavelet transforms.

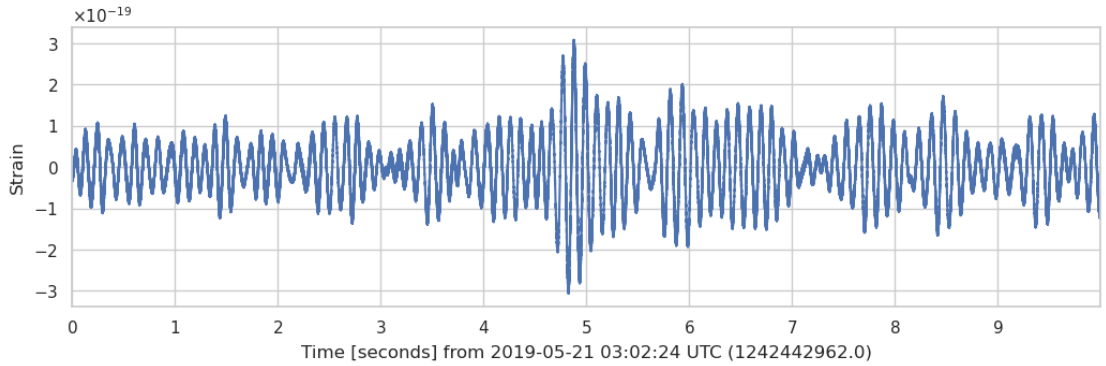

Figure 3.1: Timeseries data for LIGO Hanford for the merger GW190521 obtained using GWPy [13].

$$\tilde{x}(f) = \int_{-\infty}^{\infty} dt\, x(t) \exp(-2\pi i f t) \tag{3.1}$$

$$x(t) = \int_{-\infty}^{\infty} df\, \tilde{x}(f) \exp(2\pi i f t) \tag{3.2}$$

The conversion from time-domain to frequency-domain data is essential for analyzing and characterizing gravitational waves. In the frequency domain, the strength and shape of the gravitational wave signal can be more easily identified and distinguished from noise. Additionally, by analyzing the frequency content of the signal, it is possible to extract valuable information about the source of the gravitational waves, such as the masses and spins of the merger components that produced them.

Transforming the data into the frequency domain can often lead to spectral leakage, which happens when a signal does not fit perfectly within the frequency bins of the transform. This can cause distortion of the frequency content of the signal, making it more difficult to identify the underlying waveform.

3.2.1 Fourier Transform Windows

There are several types of Fourier transform windows used in gravitational wave analysis, including Hann, Blackman, and Tukey windows. Each of these windows has different characteristics and is suited to different types of signals.

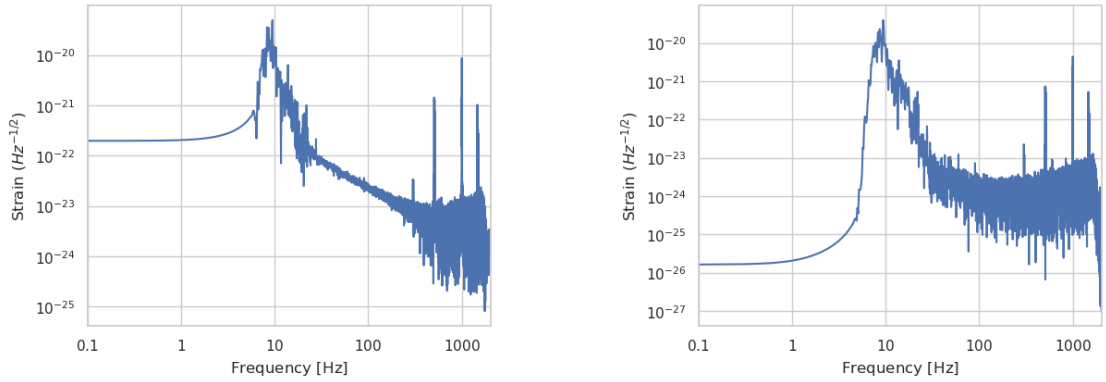

Figure 3.2: Frequency-domain data for GW190521 obtained using FFT. Left is obtained from FFT without a window function. FFT assumes that data is periodic, causing edges looking like discontinuities. Right is frequency series data after using a Hann window.

Hann Window

The Hann window is a smooth, symmetric window that tapers the edges of the signal to reduce the effect of spectral leakage. It is used by default in gravitational wave data analysis. The Hann window is defined as

$$W(n) = 0.5 - 0.5\cos\left(\frac{2\pi M}{M-1}\right) \quad \text{where } 0 \leq n \leq M-1 \tag{3.3}$$

Here, M is the number of points in the output window.

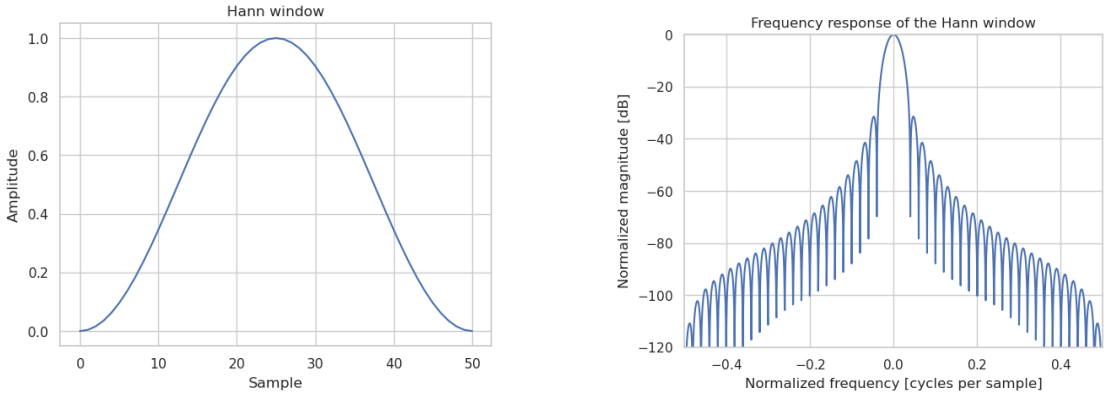

Figure 3.3: Left, the Hann window in the time domain, showing a smooth decrease to zero, which reduces the spectral power leakage. Right, its Fourier transform, showing its response in the frequency domain. Taken from [**scipyhann**].

Blackman Window

The Blackman window is a more complex window that provides a greater level of suppression of spectral leakage. It has a higher side-lobe suppression ratio than the Hann window but can introduce more ripple in the frequency domain.

$$W(n) = 0.42 - 0.5\cos\left(\frac{2\pi n}{M}\right) + 0.08\cos\left(\frac{4\pi n}{M}\right) \tag{3.4}$$

Here, M is the number of points in the output window.

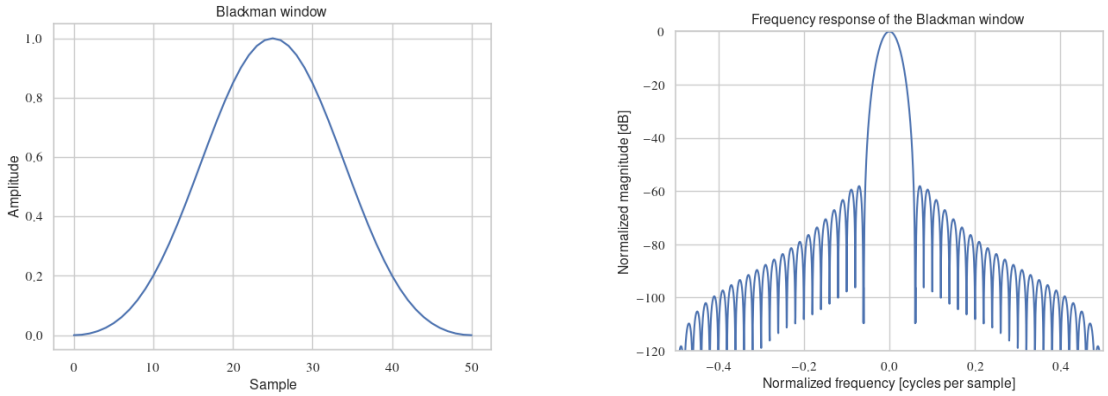

Figure 3.4: Left, the Blackman window in the time domain. Right, its Fourier transform, showing its response in the frequency domain. Taken from [14].

3.3 Practical Computation of PSD

The power spectral density of the noise in the data is estimated using the Welch method, which divides the data into overlapping segments, applies a window function to each segment, and averages the resulting periodograms. The overlap is taken as 50% by default, and the window is the Hann window. The periodogram of each segment is computed using the Fourier transform, and then the periodograms are averaged to obtain the final PSD estimate. The choice of segment length and overlap determines the trade-off between the frequency resolution and the noise variance of the PSD estimate. Longer segments provide better frequency resolution, while shorter segments reduce the variance of the estimate. The choice of window function also affects the accuracy of the estimate, as different windows have different spectral properties.

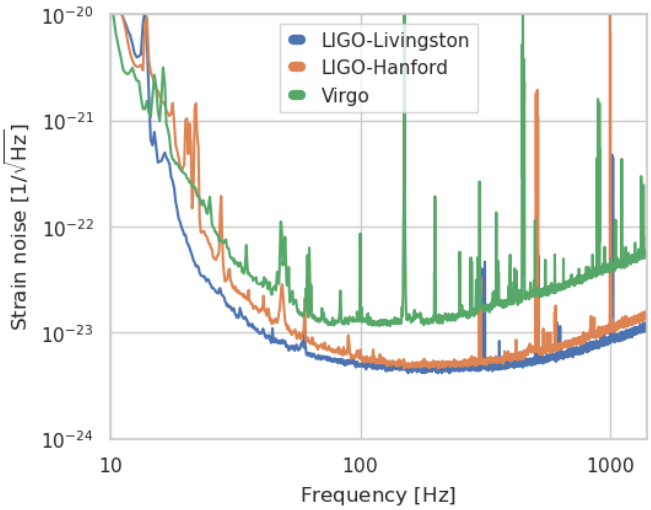

Figure 3.5: Power spectral density for the 3 detectors, represented in the range 10 Hz to 1024Hz and build for the 512s of data centered on the GW190521 event.

The analytical forms of the PSDs for twin-LIGO, Virgo, and our proposed deci-hertz detector are given in Table 2.1.

3.4 Generating Waveforms

Throughout this work, the approximant used is `IMRPhenomD`, which is a frequency domain waveform specific to binary black holes. `IMRPhenomD` is a phenomenological model that assumes aligned spins and has been tuned to a lot of simulated mergers. We define a function based on `get_fd_waveform` to generate the signals for our analysis. The outputs of this function are the sample frequencies and the plus and cross polarizations of the signal. Frequency domain waveforms are generated to reduce computational costs.

It is possible to go from the time domain to the frequency domain by the application of the Fourier transform, with the `timeseries.to_frequencyseries()` function. It is also possible to go back to a time series by the application of the inverse Fourier transform, with the `frequencyseries.to_timeseries()` command. Although the frequency domain often helps with computation, we have a better view of the evolution of the system in the time domain.

$$h \propto \frac{\mathcal{M}^{5/6}}{D_L} \tag{3.5}$$

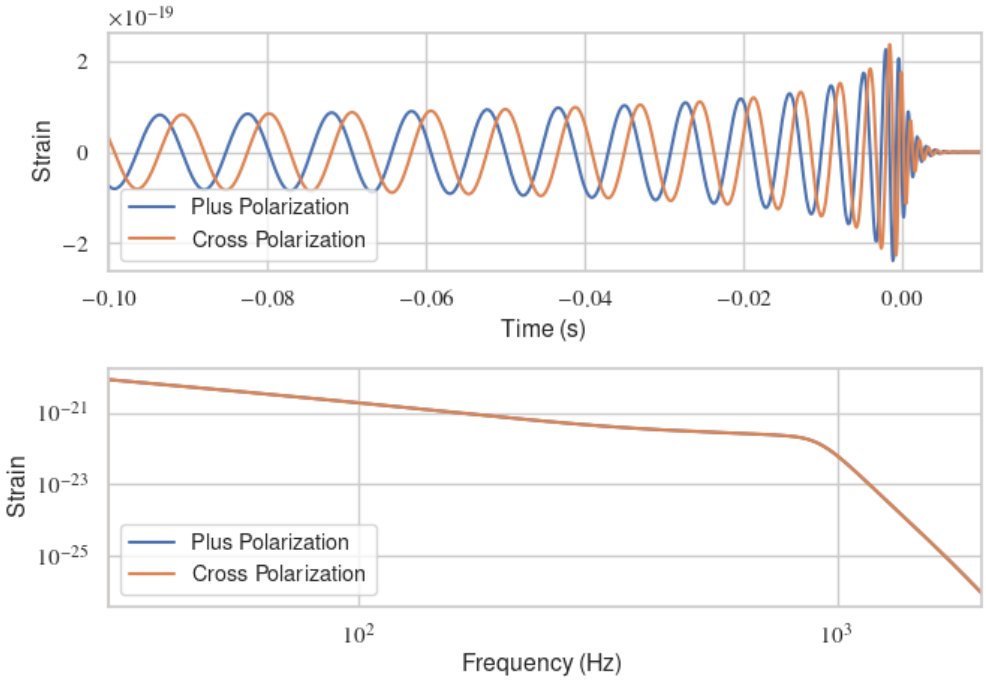

Figure 3.6: Waveforms for a system of total mass $20M_\odot$ generated using `IMRPhenomD`. Top shows the time domain signal, bottom shows frequency domain signal. Top: The amplitude and frequency increase slowly for the inspiral, followed by the merger, where the amplitude is maximum and the frequency is so high that the oscillations cannot be separated. Finally, we see the ring-down, where we have a fast decrease of the amplitude before it goes to zero.

3.5 Matched Filtering

Matched filtering is used for detecting and characterizing gravitational wave signals buried in noisy data. It involves cross-correlating the detector data with a template waveform that describes the expected shape of the signal. To understand matched filtering, it is important to learn about cross-correlation.

The cross-correlation function for two signals $h(t)$ and $n(t)$ is defined by

$$R_{hn}(\tau) = h(t)n(t-\tau) \tag{3.6}$$

R_{hn} expresses the statistical relation existing between the two signals at two different moments in time.

The matched filter SNR between a signal $s(f)$ and a template $h(f)$ for a PSD $S_n(f)$ as given in [15] is

$$(s|h)(t) = 4\mathrm{Re}\int_{f_{low}}^{f_{high}} \frac{\tilde{s}(f)\tilde{h}^*(f)}{S_n(f)} e^{2\pi i f t}\mathrm{d}f \tag{3.7}$$

3.5.1 Generating Template Waveforms

To perform matched filtering, a library of template waveforms is generated, each describing a possible gravitational wave signal that the detector may observe. This work uses the approximant `IMRPhenomD` to generate these templates for the twin-LIGO, Virgo, and the proposed deci-hertz detectors. These waveforms are then shifted using `cyclic_time_shift` so that the merger is approximately at the first bin of the data.

3.5.2 Signal Injection

Matched filtering is the optimal method to detect known signals in Gaussian noise. Signals are created as described in section 3.4 for a population of binary black holes. These signals are injected into Gaussian noise corresponding to the PSDs of each detector.

3.5.3 PSD for Injected Noise

PSDs for each of the LIGO, Virgo and the proposed deci-hertz detectors are calculated using the Welch method as described in section 3.3. This is then interpolated onto a new frequency grid to match the injected data. The interpolation is performed using the cubic spline method, which produces a smooth, continuous curve that passes through all of the original PSD values. This is followed by truncating the PSD by filtering the data in the frequency domain, by first applying a smoothing window to the PSD values to reduce the effects of noise and improve the stability of the filtering. Then the inverse of the PSD is computed and a high-pass filter is applied to the data, which suppresses noise below the specified cutoff frequency.

3.5.4 Evaluation of σ

σ^2 is used to characterize the noise in the LIGO detectors and to estimate the sensitivity of the detectors to gravitational waves. The lower the value of σ^2, the less noisy the detector is. In this study, we will be conducting zero noise injections, so σ will help us quantify how loud our signal is.

It is defined as the unnormalised matched filter of the input waveform $\tilde{h}$ with itself.

$$\sigma^2 = (h|h) \implies \sigma = \sqrt{(h|h)} \tag{3.8}$$

Here, the inner product of two quantities a and b for one-sided PSD $S_n(|f|)$ (equation (2.4)) is defined as

$$(a|b) = \int_{-\infty}^{\infty} df \frac{\tilde{a}^*(f)\tilde{b}(f) + \tilde{a}(f)\tilde{b}^*(f)}{S_n(|f|)} \tag{3.9}$$

If both a and b are real functions of time,

$$(a|b) = 2\int_{-\infty}^{\infty} df \frac{\tilde{a}(f)\tilde{b}^*(f)}{S_n(|f|)} \tag{3.10}$$

From the definition of inner product in equation (3.10) and the definition of σ^2 in equation (3.8), it can be written

$$\sigma^2 = 2\int_{-\infty}^{\infty} df \frac{\tilde{h_c}^*(f)\tilde{h_c}(f)}{S_h(|f|)} \tag{3.11}$$

$$\sigma = \sqrt{2\int_{-\infty}^{\infty} df \frac{\tilde{h_c}^*(f)\tilde{h_c}(f)}{S_h(|f|)}} \tag{3.12}$$

3.5.5 Matched Filtering in Action

Next, the data is filtered using a series of matched filters, each corresponding to one of the template waveforms in the library. The output of each matched filter is a time series of values that represents the strength of the match between the data and the corresponding template waveform. From this data, the peak SNR value is evaluated.

3.5.6 Signal-to-Noise Ratio

The strength of the match between the data and the template waveform is quantified using a signal-to-noise ratio (SNR) as defined in equation (3.7). A time series

of SNR is generated from which the peak SNR is calculated. Gravitational wave signals with a high SNR are more likely to be real signals than those with a low SNR. The threshold for a signal to be classified as detected used in this work is 8. For the scope of this work, σ is evaluated to quantify the loudness of the signal in zero noise. The terms σ and SNR are used interchangeably henceforth.

3.6 Signal Consistency Tests

A chi-square test is used to have a numerical estimate of the quality of the fit. This test was first used to veto some peaks made by noise rather than a signal. In this case, the chi-square test differentiates the peaks due to noise from those due to a real gravitational wave signal. The peaks due to noise arise when there is a glitch. Often, when the computations are done, especially in the case of matched filtering, the noise is assumed to be Gaussian. In fact, the noise is not totally Gaussian, and, in some cases, peaks of noise arise and have a Poisson-like distribution.

4 Methods

This work follows the pipeline described in chapter 3 to study the population distribution of black holes in the deci-hertz band. Chapter 3 discusses matched filtering techniques for signals injected into Gaussian noise, however, our analysis focuses on zero-noise injections. We aim to analyze the proportion of detectable mergers with a hypothetical deci-hertz observatory and LIGO+Virgo working in conjugation. For this, a population of binary black holes is created using the `bilby` pipeline. The bulk of the analysis is carried out using the `PyCBC` package [15].

4.1 Generating a BBH Population

We use the `bilby.core.prior` module to generate a prior dictionary defining our black hole population distributions. This prior dictionary is then used to generate a population of 1000 black holes for our analyses.

The primary mass follows a power law with an index -2.35. This is obtained from the Salpeter mass distribution, which is a statistical model that describes the distribution of masses for a population of stars. The Salpeter mass function is characterized by a high number of low-mass stars and a small number of high-mass stars. It can also be used to describe the distribution of masses for black holes, which are compact objects formed by the gravitational collapse of massive stars. This is because the process of black hole formation is closely tied to the initial mass of the progenitor star, which determines the mass of the black hole that is formed. In fact, recent observations of merging black holes and neutron stars by LIGO and Virgo have confirmed the presence of a population of compact objects with masses that are consistent with a Salpeter-like distribution. The Salpeter mass function is a power-law distribution of the form

$$N(m)\mathrm{d}m \propto m^{-\alpha} \tag{4.1}$$

where $N(m)$ is the number of bodies with mass between m and $m + \mathrm{d}m$, and

Parameter	Distribution	Minimum	Maximum
m_1	PowerLaw	5	500
m_2	Constraint	5	500
q	Uniform	0.1	1
a_1	Uniform	0	0.99
a_2	Uniform	0	0.99
ϕ_{12}	Uniform	0	2π
ϕ_{jl}	Uniform	0	2π
d_L	Uniform	10	4000
ϕ_c	Uniform	0	2π
ψ	Uniform	0	π
α	Uniform	0	2π
δ	Cosine	—	—

Table 4.1: Population parameters for the generated population. The parameters are mass 1 (m_1), mass 2 (m_2), mass ratio (q), spin amplitudes 1 and 2 (a_1, a_2), spin vector azimuthal angle (ϕ_{12}), precession angle about angular momentum (ϕ_{jl}), luminosity distance (d_L), phase (ϕ_c), right ascension (α) and declination (δ).

α is the slope of the power law. The Salpeter IMF has a slope of $\alpha = 2.35$ which means that it predicts that there are many more low-mass stars than high-mass stars in a stellar population. This distribution is extended to our study.

A prior is placed on the luminosity distance using `UniformSourceFrame`, which generates a uniform prior distribution over the source frame parameters of a gravitational wave signal. When a gravitational wave signal is emitted by a source, it is redshifted as it travels through the expanding universe. This prior is useful when we have no prior knowledge about the location of the source and want to place a uniform prior on the luminosity distance of the source in the source frame, which is a reference frame that moves with the source, and in this frame, the source is at rest. Placing a uniform prior on the luminosity distance in the source frame ensures that we are not biasing our inference towards sources at lower or higher redshifts.

Uniform priors are placed on other source parameters which are then used to generate the samples for this study. This means that the prior distribution does not favor any particular value of the parameter, and it can be interpreted as expressing a lack of prior knowledge or bias about the parameter. The distributions of all source parameters of this population are given in Fig. 4.3.

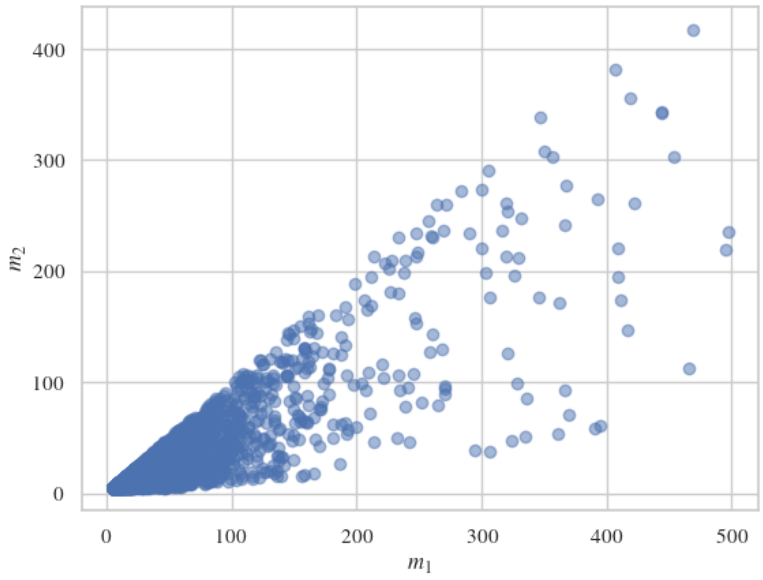

Figure 4.2: Power law distribution of masses with index $\alpha = -2.35$.

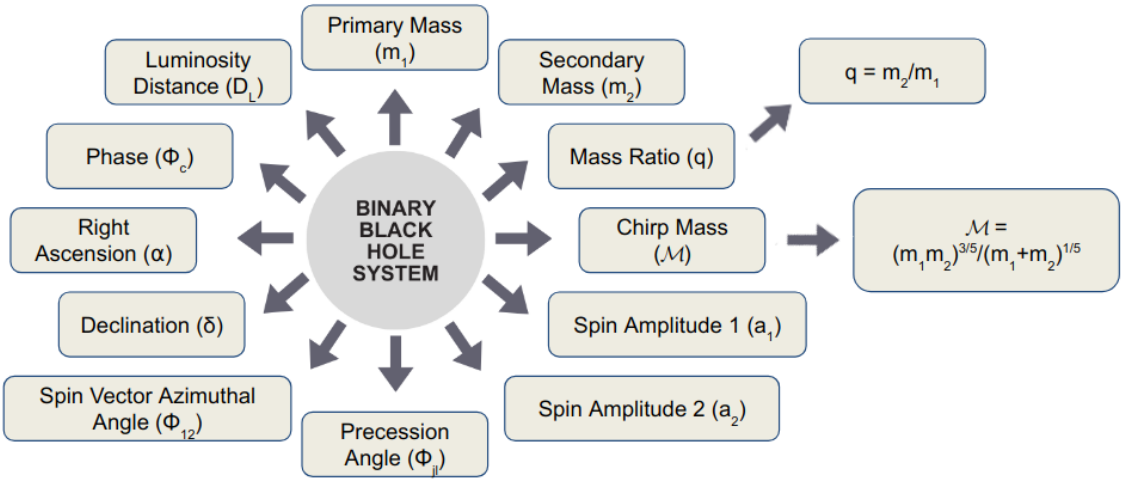

Figure 4.1: A pictorial representation of parameters that represent the intrinsic as well as intrinsic properties of a binary black hole. Created using Canva.

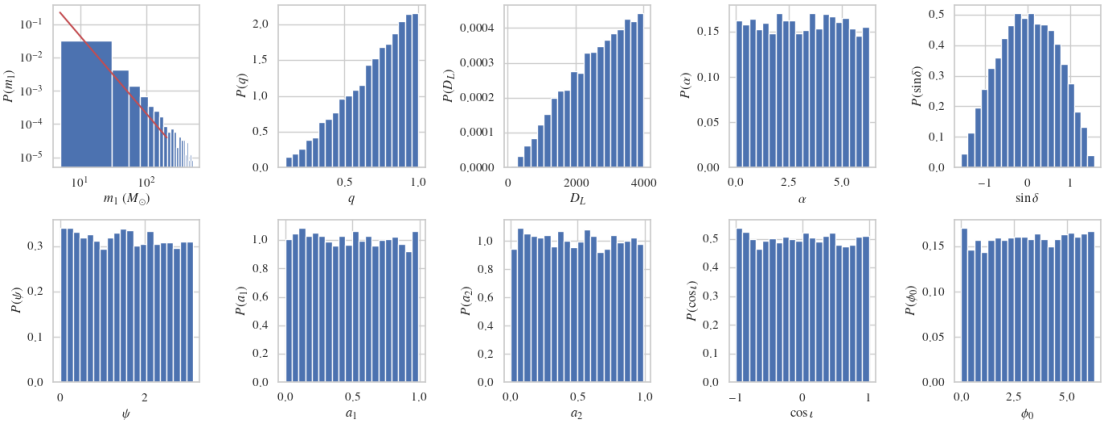

Figure 4.3: Distribution of all parameters of the generated population. The bounds on the parameters are given in Table 4.1.

4.2 Generating Noise

As discussed in section 3.3, the sensitivity curves for LIGO+Virgo and the deci-hertz observatory are obtained (shown in Fig. 2.4). For LIGO+Virgo, we use the A+ design target sensitivity curves for the fifth observing run (O5) provided at LIGO DCC [11]. The sensitivity curve for the deci-hertz observatory is empirically determined, the Python script for which can be found here [12]. Frequency domain Gaussian noise is generated corresponding to these PSDs with the `PyCBC` module.

4.2.1 Sampling Rate and Resolution

The sampling rate is taken to be 4096Hz for twin-LIGO, Virgo, and the deci-hertz observatory. LIGO raw data is sampled at 16384Hz, which captures signal frequency up to $f_{Nyquist} = 8192$Hz. For the scope of this work, the data is down-sampled to avoid computationally expensive calculations. A segment of 32s is considered ($\Delta f = 1/32$). The lower frequency cutoff for LIGO is placed at 10Hz [16], and that for the deci-hertz observatory is placed at 0.05Hz [17].

Detector	Sampling rate	Δf	Frequency cutoff (f_{low})	PSD length
LIGO+Virgo	4096	1/32	10	65537
Deci-hertz	4096	1/32	0.05	65537

Table 4.2: Parameters used for generation of PSDs and then noise from [11].

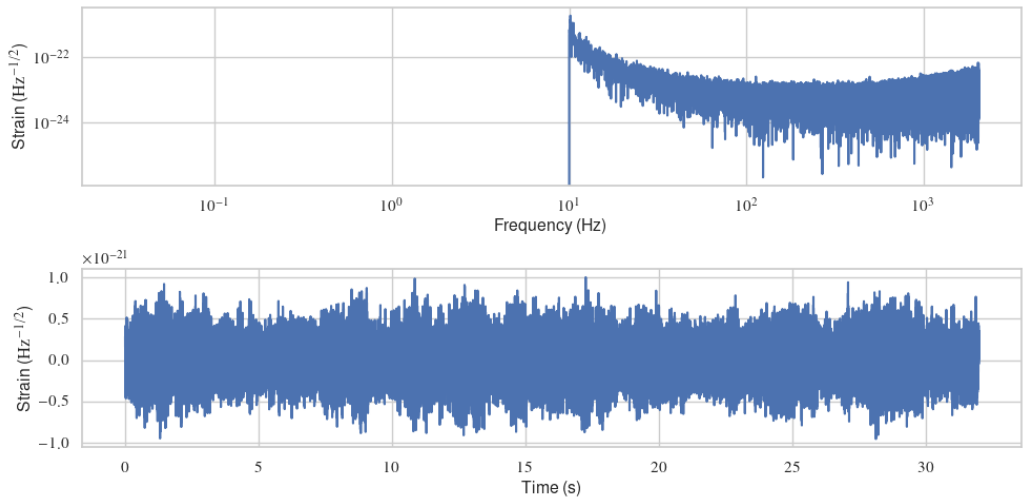

Figure 4.4: Gaussian noise in frequency (top) and time (bottom) domains generated from the LIGO Hanford PSD.

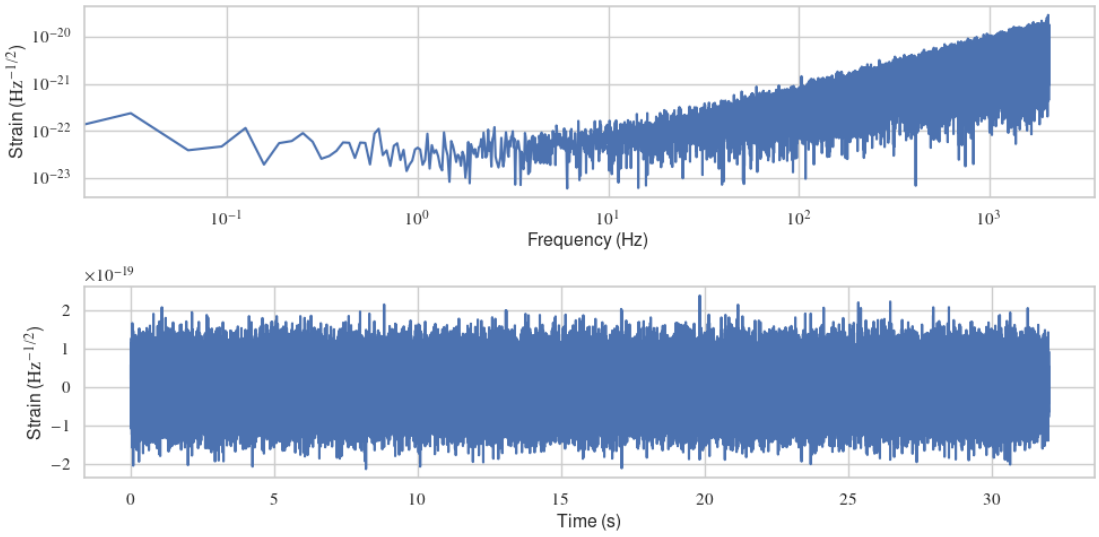

Figure 4.5: Gaussian noise in frequency (top) and time (bottom) domains generated from the deci-hertz PSD.

4.3 Generating Signals

Frequency domain signals for the black hole population are generated using `IMRPhenomD` following a similar methodology as discussed in section 3.4. This generates

both plus (h_+) and cross ($h_\times$) polarizations. The antenna pattern functions for LIGO Hanford are taken from [18]. Antenna pattern function for the deci-hertz observatory is taken as $\sqrt{4/5}$ [19].

For the scope of this work, we conduct no-noise injections and quantify the *loudness* of the signal for the given detector PSDs. This estimation is made by σ, which is defined in equation (3.8). The computational cost of conducting matched filtering for a template bank for our population is a limitation for this work. The higher limit on the frequency is placed at

$$f_{high} = \frac{0.1}{M_T m_1 (1+q)} \tag{4.2}$$

where M_T is the mass of the Sun in seconds, m_1 is the primary mass and q is the mass ratio.

4.4 Evaluating SNR (σ)

The loudness of the generated signals with both the HLV and deci-hertz PSDs is calculated using the `PyCBC` module. A signal is classified as detectable in a frequency band if the SNR (σ) obtained is greater than 8.

4.5 Example Events

In this section, we demonstrate how multiband detection could work with two example events— stellar-mass black holes and intermediate-mass black holes.

4.5.1 Stellar-Mass Black Holes

The binary we are looking at consists of two black holes with masses $m_1 = 15M_\odot$ and $m_2 = 14M_\odot$, at a distance of $D_L = 3000$MPc. The SNR obtained for HLV and the deci-hertz detector is shown in Table 4.3.

	HLV	Deci-hertz
SNR	14	200

Table 4.3: SNRs of the stellar-mass BBH example binary in different detectors.

4.5.2 Intermediate-Mass Black Holes

We consider a binary from our population with $m_1 = 150M_\odot$ and $m_2 = 120M_\odot$, at a distance $D_L = 2525$MPc. The SNR obtained for HLV and the deci-hertz detector is shown in Table 4.4.

	HLV	Deci-hertz
SNR	84	1436

Table 4.4: SNRs of the intermediate-mass BBH example binary in different detectors.

5 Results and Discussion

5.1 Inference

We observe that our proposed deci-hertz observatory is able to detect 1000 out of 1000 simulated mergers, whereas, the LIGO Hanford detector detects only 607 with A+ design sensitivity, as shown in Table 5.1. Both LIGO Hanford and the deci-hertz observatory show an SNR value of >8 for detections of stellar-mass black hole mergers (Table 4.3) and intermediate-mass black hole mergers (Table 4.4). Upon careful examination, it is found that the intermediate-mass merger generates a nearly six-fold higher signal-to-noise ratio (SNR) for both the LIGO Hanford and the deci-hertz detector. Interestingly, the LIGO Hanford detector exhibits an SNR below 8 for stellar-mass mergers with low component masses, which is inconsistent with the expected trend. However, it displays significantly higher SNR values for intermediate-mass mergers, which indicates a discrepancy between the observed and anticipated behavior of the detector.

SNR > 8 events	HLV	Deci-hertz
Out of 1000 events	607	1000

Table 5.1: Number of events with an SNR > 8 in the different detectors out of a cosmological distribution of 1000 binary black holes.

Figure 5.1 illustrates that the signal-to-noise ratio (SNR) values obtained from the deci-hertz and LIGO detectors follow a Gaussian distribution, but with a slight skew towards higher SNR values. We postulate that this deviation from a perfectly symmetrical distribution may be attributed to the presence of outliers in the analysis.

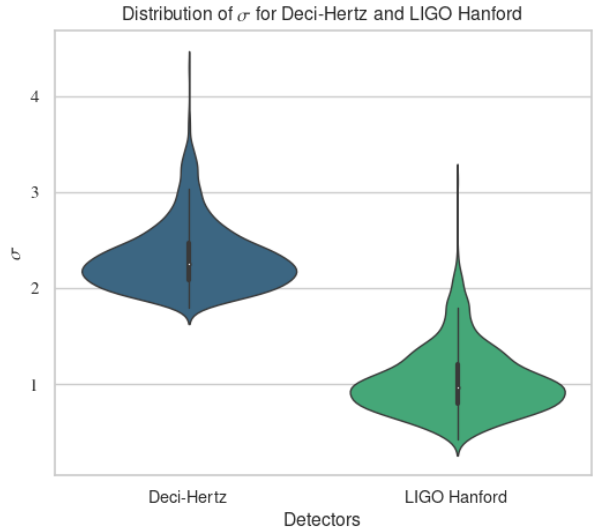

Figure 5.1: Violin plots representing the distribution of SNRs for both LIGO Hanford and a deci-hertz observatory. The plots are made in logscale for comparison. It can be seen that the SNRs follow a normal distribution slightly skewed towards higher values. This is because of outliers.

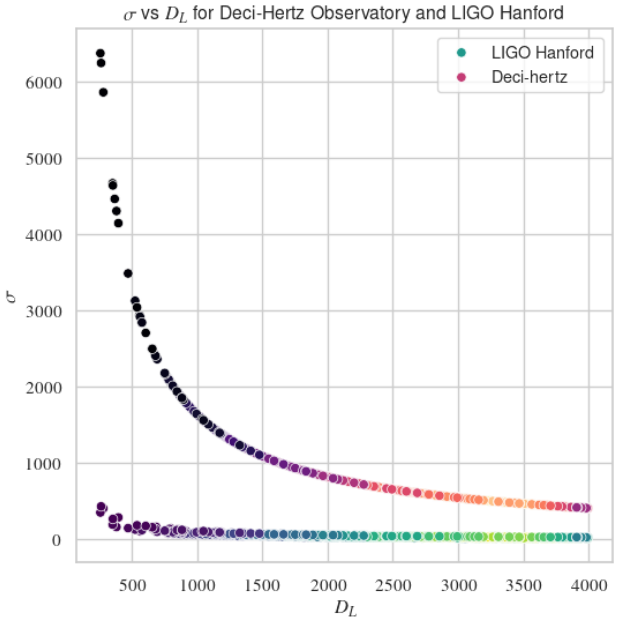

Figure 5.2: Comparison of SNR (σ) vs luminosity distance for fixed parameters for the proposed deci-hertz observatory and LIGO Hanford. Color gradient represents counts.

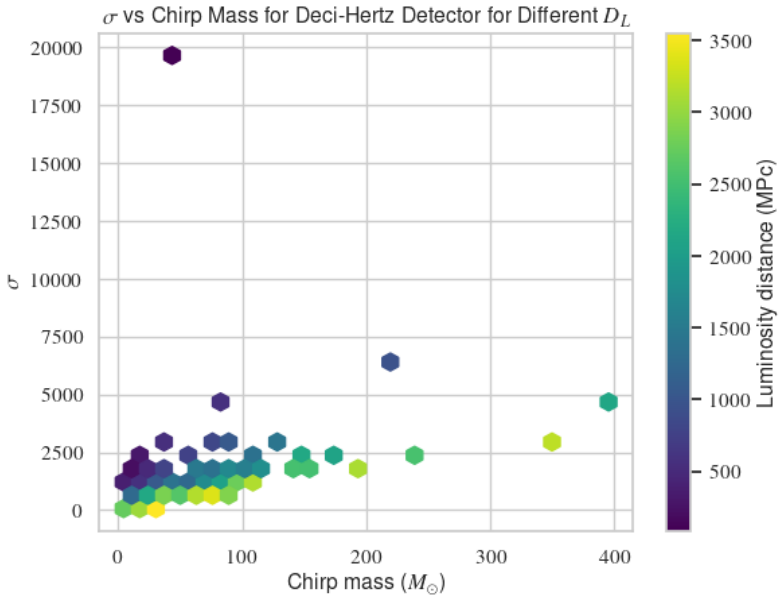

Figure 5.3: SNR (σ) vs chirp mass for our proposed deci-hertz observatory. Color scale represents the luminosity distance.

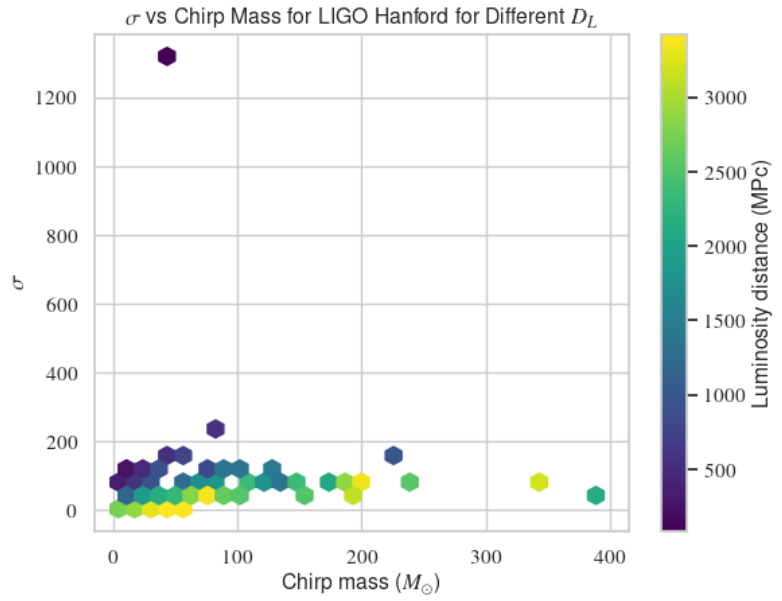

Figure 5.4: SNR (σ) vs chirp mass for our proposed deci-hertz observatory. Color scale represents the luminosity distance.

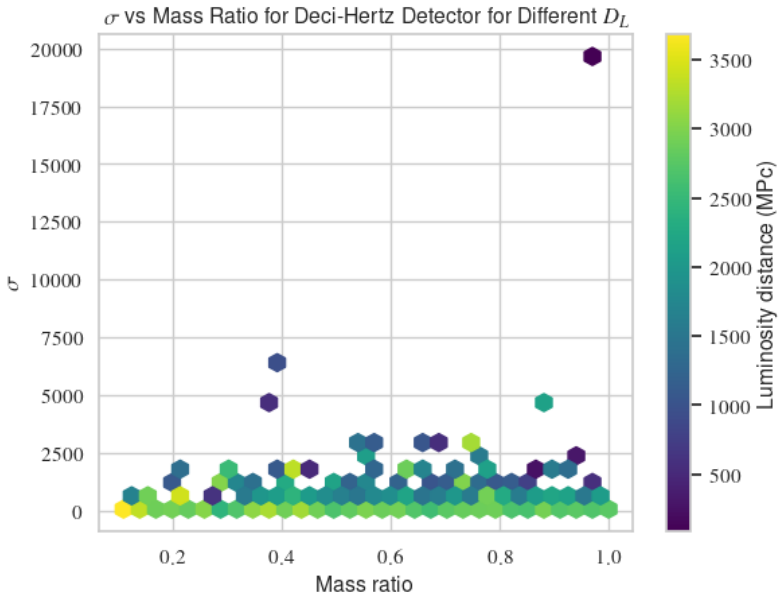

Figure 5.5: SNR (σ) vs mass ratio (q) for the proposed deci-hertz detector. Color scale represents luminosity distance (D_L).

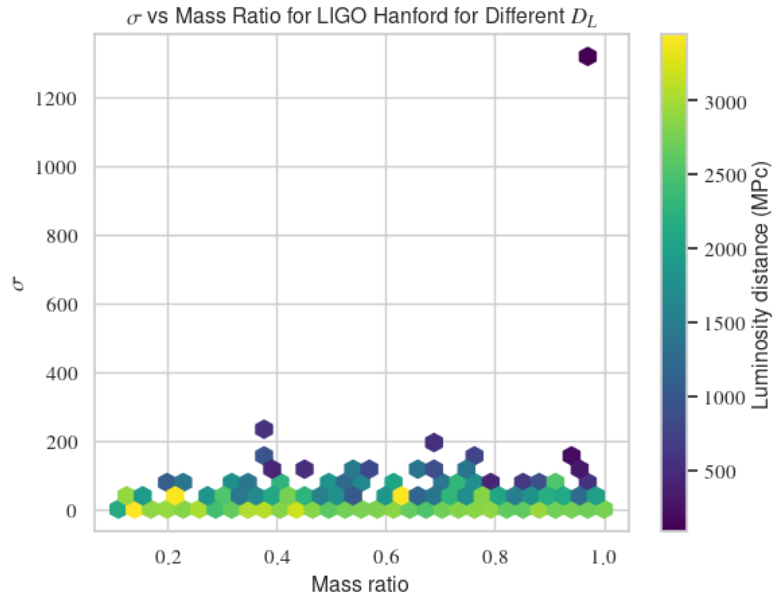

Figure 5.6: SNR (σ) vs mass ratio (q) for LIGO Hanford. Color scale represents luminosity distance (D_L).

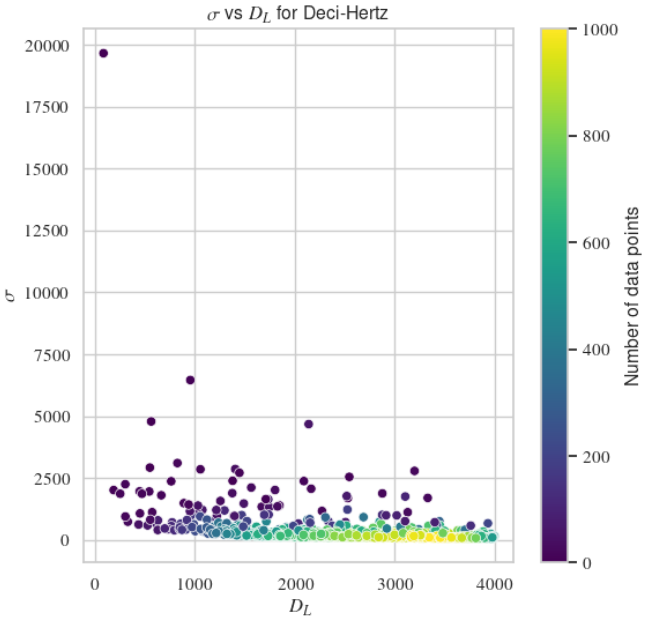

Figure 5.7: SNR (σ) vs luminosity distance for our proposed deci-hertz observatory. Color gradient represents the density of points.

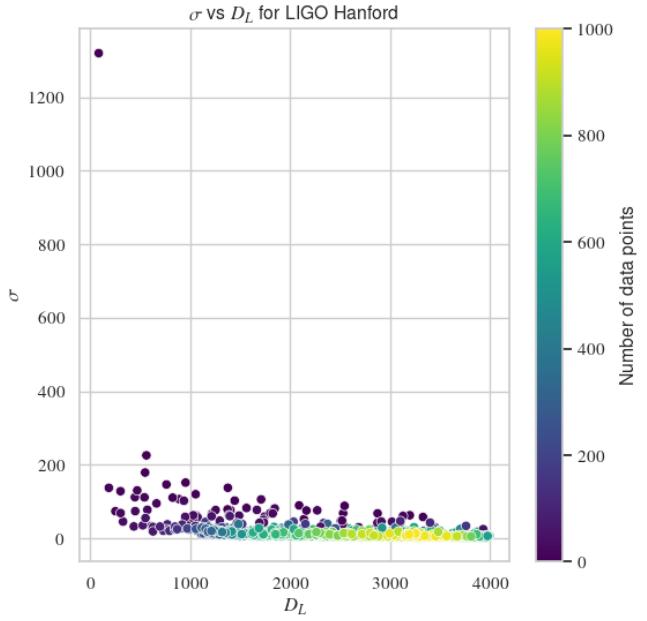

Figure 5.8: SNR (σ) vs luminosity distance for LIGO Hanford. Color gradient represents the density of points.

Figure 5.2 shows that the proposed deci-hertz observatory has a higher SNR (σ) in comparison to LIGO Hanford for varying luminosity distances. Despite the decrease in the SNR with increasing luminosity distance, the deci-hertz observatory consistently outperforms LIGO Hanford in terms of the SNR. This difference is particularly prominent for binary systems with lower luminosity distances.

After examining the figures 5.3 and 5.4, which depict the relationship between SNR and chirp mass for the deci-hertz detector and LIGO Hanford, we observed a positive correlation between the two parameters. This observation aligns with [20] that SNR is directly proportional to the chirp mass to the power of 5/6. However, distance to the source dominates the relationship, and the SNR for binaries with greater distances continues to be low. This finding highlights the critical role of the chirp mass parameter in the detection of binary systems using gravitational wave detectors.

On studying figures 5.5 and 5.6, we observe that the SNR is not affected by the mass ratio of the system and remains constant for all mass ratios at a given distance. As depicted in the figures, the SNR increases in increments as the distance decreases, but remains relatively stable for different mass ratios at the same distance. The SNR is least for the farthest systems as anticipated.

Figures 5.7 and 5.8 depict the relationship between SNR and luminosity distance for varying masses. The color scale on these plots represents counts. The decreasing nature of the plot is still retained and is visible from the plots.

5.2 Conclusion

The present study reinforces that a signal originating from a binary system at a shorter distance has a higher signal-to-noise ratio (SNR) compared to a system with a greater luminosity distance, which is consistent with the anticipated trend. As the wavefront propagates further from the source, the amplitude of the signal detected at the receiving end diminishes, resulting in lower SNR values for distant sources. Furthermore, the results show a positive correlation between the SNR and the chirp mass of the system, but the distance still dominates and keeps the SNR low. Remarkably, we demonstrate that the proposed deci-hertz observatory has a 100% detectability rate and outperforms the current hecto-hertz ground-based detectors. The deci-hertz observatory has higher detection capabilities, particularly for higher-mass binary systems, and can capture a longer segment of the event leading to the merger. The addition of a deci-hertz observatory in the gravitational wave detector network will, therefore, enable us to investigate unprobed sources of gravitational waves.

5.3 Limitations and Future Directions

The progress of this study was greatly limited by the high computational cost of executing the pipelines. As a result, several assumptions were made to enable feasible completion of this work. To obtain more accurate inference, it is recommended to increase the population size beyond the current sample of 1000. Furthermore, the power spectral densities (PSDs) for both LIGO detectors and the deci-hertz detector have been downsampled to 4096 Hz. The analysis presented in this work was conducted with zero-noise injections, which allowed for computation of σ. However, for more realistic results, it is necessary to include actual noise in future studies. The limitations of the `IMRPhenomD` model prevented inclusion of mergers with mass ratios in the range of 10^2-10^4, commonly referred to as intermediate mass ratio inspirals (IMRIs). Lastly, the analysis was limited to the LIGO Hanford detector from the LIGO and Virgo collaborations, and should be conducted with all three detectors.

Bibliography

[1] B. P. Abbott et al. "Observation of Gravitational Waves from a Binary Black Hole Merger". In: *Phys. Rev. Lett.* 116 (6 Feb. 2016), p. 061102. DOI: 10.1103/PhysRevLett.116.061102. URL: https://link.aps.org/doi/10.1103/PhysRevLett.116.061102.

[2] The LIGO Scientific Collaboration et al. "A guide to LIGO-Virgo detector noise and extraction of transient gravitational-wave signals". In: *Classical and Quantum Gravity* 37.5 (Mar. 5, 2020), p. 055002. ISSN: 0264-9381, 1361-6382. DOI: 10.1088/1361-6382/ab685e. arXiv: 1908.11170[astro-ph, physics:gr-qc]. URL: http://arxiv.org/abs/1908.11170 (visited on 03/16/2023).

[3] The LIGO Scientific Collaboration et al. "GW190521: A Binary Black Hole Merger with a Total Mass of $150 ~ M_{\odot}$". In: *Physical Review Letters* 125.10 (Sept. 2, 2020), p. 101102. ISSN: 0031-9007, 1079-7114. DOI: 10.1103/PhysRevLett.125.101102. arXiv: 2009.01075[astro-ph, physics:gr-qc]. URL: http://arxiv.org/abs/2009.01075 (visited on 04/24/2023).

[4] Karsten Danzmann and the LISA study team the. "LISA: laser interferometer space antenna for gravitational wave measurements". In: *Classical and Quantum Gravity* 13.11 (Nov. 1996), A247. ISSN: 0264-9381. DOI: 10.1088/0264-9381/13/11A/033. URL: https://dx.doi.org/10.1088/0264-9381/13/11A/033 (visited on 04/20/2023).

[5] C Moore, Robert Cole, and C Berry. *** Gravitational Wave Sensitivity Curve Plotter ** — gwplotter.com*. http://gwplotter.com/. [Accessed 24-Apr-2023].

[6] Gregory Ashton et al. "Bilby: A user-friendly Bayesian inference library for gravitational-wave astronomy". In: *The Astrophysical Journal Supplement Series* 241.2 (Apr. 1, 2019), p. 27. ISSN: 1538-4365. DOI: 10.3847/1538-4365/ab06fc. arXiv: 1811.02042[astro-ph,physics:gr-qc]. URL: http://arxiv.org/abs/1811.02042 (visited on 04/20/2023).

[7] B S Sathyaprakash and B F Schutz. "Physics, astrophysics and cosmology with gravitational waves". In: (Mar. 2009). arXiv: 0903.0338 [gr-qc].

[8] A. Buikema et al. "Sensitivity and performance of the Advanced LIGO detectors in the third observing run". In: *Phys. Rev. D* 102 (6 Sept. 2020), p. 062003. DOI: 10.1103/PhysRevD.102.062003. URL: https://link.aps.org/doi/10.1103/PhysRevD.102.062003.

[9] Seiji Kawamura et al. "Space gravitational-wave antennas DECIGO and B-DECIGO". In: *International Journal of Modern Physics D* 28.12 (Sept. 2019). Publisher: World Scientific Publishing Co., p. 1845001. ISSN: 0218-2718. DOI: 10.1142/S0218271818450013. URL: https://www.worldscientific.com/doi/10.1142/S0218271818450013 (visited on 04/20/2023).

[10] Kevin Kuns. *Files · master · gwinc / pygwinc · GitLab — git.ligo.org*. https://git.ligo.org/gwinc/pygwinc/-/tree/master/. [Accessed 16-Apr-2023].

[11] *LIGO-T1800042-v5: The A+ design curve — dcc.ligo.org*. https://dcc.ligo.org/LIGO-T1800042/public. [Accessed 21-Apr-2023].

[12] Akshita Mittal. *GitHub - drnkyda/Minor-Project-2023 — github.com*. https://github.com/drnkyda/Minor-Project-2023. [Accessed 21-Apr-2023].

[13] Duncan Macleod et al. "GWpy: Python package for studying data from gravitational-wave detectors". In: *Astrophysics Source Code Library* (Dec. 1, 2019). ADS Bibcode: 2019ascl.soft12016M, ascl:1912.016. URL: https://ui.adsabs.harvard.edu/abs/2019ascl.soft12016M (visited on 04/24/2023).

[14] *scipy.signal.windows.blackman x2014; SciPy v1.10.1 Manual — docs.scipy.org*. https://docs.scipy.org/doc/scipy/reference/generated/scipy.signal.windows.blackman.html#scipy.signal.windows.blackman. [Accessed 23-Apr-2023].

[15] Samantha A. Usman et al. "The PyCBC search for gravitational waves from compact binary coalescence". In: *Classical and Quantum Gravity* 33.21 (Nov. 3, 2016), p. 215004. ISSN: 0264-9381, 1361-6382. DOI: 10.1088/0264-9381/33/21/215004. arXiv: 1508.02357 [astro-ph,physics:gr-qc]. URL: http://arxiv.org/abs/1508.02357 (visited on 04/22/2023).

[16] P Fritschel, D Shoemaker, and D Coyne. "Low-frequency Cutoff for Advanced LIGO". In: ().

[17] Kent Yagi. "Gravitational wave observations of galactic intermediate-mass black hole binaries with DECIGO path finder". In: *Classical and Quantum Gravity* 29.7 (Mar. 2012). Publisher: IOP Publishing, p. 075005. ISSN: 0264-9381. DOI: 10.1088/0264-9381/29/7/075005. URL: https://dx.doi.org/10.1088/0264-9381/29/7/075005 (visited on 04/21/2023).

[18] Hsin-Yu Chen et al. "Distance measures in gravitational-wave astrophysics and cosmology". In: *Classical and Quantum Gravity* 38.5 (Mar. 4, 2021), p. 055010. ISSN: 0264-9381, 1361-6382. DOI: 10.1088/1361-6382/abd594. arXiv: 1709.08079[astro-ph]. URL: http://arxiv.org/abs/1709.08079 (visited on 04/21/2023).

[19] Sayantani Datta et al. "Tests of general relativity using multiband observations of intermediate mass binary black hole mergers". In: *Physical Review D* 103.2 (Jan. 20, 2021), p. 024036. ISSN: 2470-0010, 2470-0029. DOI: 10.1103/PhysRevD.103.024036. arXiv: 2006.12137[astro-ph,physics:gr-qc]. URL: http://arxiv.org/abs/2006.12137 (visited on 04/21/2023).

[20] Curt Cutler and Éanna E. Flanagan. "Gravitational waves from merging compact binaries: How accurately can one extract the binary's parameters from the inspiral waveform?" In: *Phys. Rev. D* 49 (6 Mar. 1994), pp. 2658–2697. DOI: 10.1103/PhysRevD.49.2658. URL: https://link.aps.org/doi/10.1103/PhysRevD.49.2658.